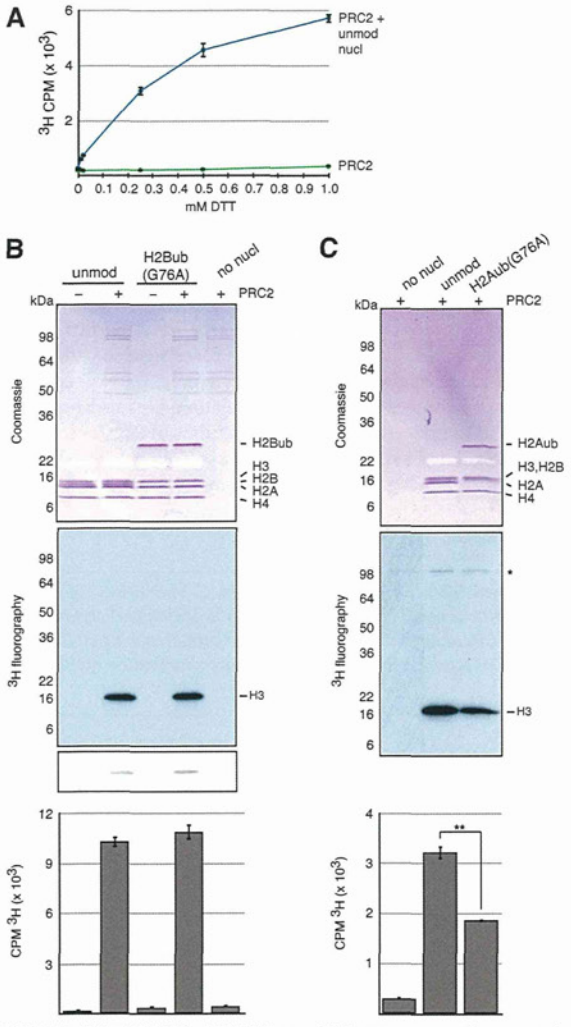

FIGURE 4. **H2Aub inhibits PRC2 MTase activity on mononucleosomes.** *A*, DTT titration of PRC2 MTase activity on unmodified mononucleosomes (*unmod nucl*) as quantitated by scintillation counting of incorporated ^{3}H. *Error bars* represent the S.D. of multiple scintillation counts. *B* and *C*, PRC2 MTase activity was tested under reducing conditions on *Xenopus* unmodified, H2Bub(G76A), and H2Aub(G76A) mononucleosomes. Representative experiments are shown. Reactions were separated by SDS-PAGE and Coomassie Blue-stained, and activity was assessed by fluorography. In *B*, a short exposure is shown below a longer exposure. In *C*, automethylation activity is indicated (*). Activity was also assessed by scintillation counting of incorporated ^{3}H into a fraction of each reaction (one-half in *A* and one-fourth in *B*). *Error bars* indicate the S.D. of multiple scintillation counts of the same reaction. In *C*, **, $p <$ 0.0001 (Student's paired test).

ibly inhibited PRC2 MTase activity (Fig. 4*C*). This was an unexpected result because both H3K27me and H2Aub are transduced by PRC2 and PRC1, respectively, with well established roles in gene repression. However, several recent publications provide evidence that the functional link between H2Aub and transcriptional repression is not as clear as was once thought (40–42), and these will be discussed further below.

	H3K79me	H3K4me	H3K27me
H2BK120ub	⊕ Dot1L ⊕ Dot1L	⊕ Set1	○ PRC2
H2AK119ub	○ Dot1L	⊖ MLL3	⊖ PRC2

FIGURE 5. **Summary of enzymatic cross-talk relationships between histone monoubiquitylation and methylation.** *Left*, histone monoubiquitylation sites known to directly influence MTase activity directed toward the indicated histone methylation sites (*top*) are indicated. *Inside*, the relevant MTase and the type of cross-talk observed are indicated. ⊕, the ubiquitylated histone directly stimulates the indicated MTase; ⊖, inhibition; ○, no detected stimulation or inhibition. The results presented here and those published by others (see text) are colored in *blue* and *black*, respectively.

DISCUSSION

Cross-talk between histone PTMs may have evolved as a way to amplify, buffer, and integrate diverse signals impinging on chromatin. Elucidating which PTMs "talk" to each other, which do not, and via what mechanisms is critical in our quest to understand cellular memory, development, and disease. To study direct enzymatic cross-talk relationships between PTMs, the use of highly defined *in vitro* chromatin templates is critical (28). Here, we utilized chemically defined monoubiquitylated histones to generate a set of mononucleosomal substrates for MTase assays to investigate novel functions of histone ubiquitylation and to shed light on the plasticity/specificity of cross-talk with histone MTases (Fig. 5).

In landmark papers, H2Bub was shown to be an *in vivo* requisite for methylation of H3K79 by Dot1 (9, 11). Careful subsequent studies using nucleosomes with site-specifically installed monoubiquitin revealed that H2BK120ub directly stimulates Dot1 MTase activity (15). Interestingly, H2BK120ub is not unique in its ability to cross-talk with Dot1L-mediated H3K79 methylation. Ubiquitylation at several other sites on the nucleosome axial face and on the radial edge can also stimulate Dot1L activity (24, 32). From these data, it is clear that Dot1L stimulation is relatively plastic with regard to the position of histone monoubiquitylation. Using a disulfide-mediated approach, we installed monoubiquitin at position 119 of H2A to test whether H2Aub, the most abundant ubiquitylated species in metazoan chromatin, could influence Dot1L MTase activity on mononucleosomes. Our results clearly show that the observed plasticity of the ubiquitylation site for Dot1L stimulation *in vitro* does not extend to H2Aub (Fig. 3*C*). Thus, even though H2Aub is a relatively abundant mark in mammalian systems, it seems likely that its biological function is not linked to H3K79 methylation and downstream events.

Most studies of the function of H2Bub in metazoans have focused on its role in transcriptional activation (43). Although the steady-state H2Bub level correlates well with the most highly expressed genes genome-wide (44), *in vivo* depletion of RNF20 (E3 ligase for H2BK120) and near abolishment of H2Bub revealed a subset of genes repressed by RNF20 (45). Surprisingly, genes repressed by RNF20 were found to be associated with higher levels of H2Bub than genes activated by RNF20. These data raise the possibility that H2Bub may be

involved in transcriptional repression in some chromatin contexts.

Given that H2Bub dramatically and directly stimulates the evolutionarily unrelated MTases Dot1 and Set1, we wondered whether the ability of H2Bub to stimulate MTases is restricted to MTases involved in active transcription (*e.g.* H3K4me and H3K79me) or if it extends to MTases involved in transcriptional repression (such as PRC2). *In vitro* PRC2 MTase assays revealed no cross-talk, in either a stimulatory or inhibitory direction, between H2Bub and PRC2-mediated H3K27me (Fig. 4*B*). Based on these results, it is unlikely that putative H2Bub-mediated transcriptional repression, as observed in genome-wide studies (45), is caused by direct stimulation of PRC2 activity. Going forward, it will be interesting to understand at the molecular/structural level how H2Bub selectivity stimulates MTases Dot1L and Set1 but not PRC2.

Although H2Aub is typically understood to cooperate with PRC2-mediated H3K27 methylation in transcriptional repression, we found that H2Aub produced a modest but reproducible inhibition of PRC2 activity *in vitro* (Fig. 4*C*). One more trivial explanation for our finding might be that the relatively close proximity of H2AK119ub to H3K27 in the nucleosome (Fig. 1*B*) may simply sterically hinder PRC2 MTase activity. Although this possibility cannot be ruled out by our studies, recently published data from several groups suggest that the widely accepted link between H2Aub and transcriptional repression may not be so straightforward (40–42).

Eskeland *et al.* (42) showed that the H2A E3 ligase activity of Ring1B is dispensable for transcriptional repression of Polycomb target genes and for long-range chromatin compaction of *Hox* gene clusters *in vivo*. In light of our *in vitro* results, it would be of interest to know whether cells with catalytically null Ring1B have attenuated or otherwise misregulated activation of *Hox* genes during differentiation.

Scheuermann *et al.* (41) identified a novel Polycomb repressive complex in *Drosophila* with H2A deubiquitinase activity, PR-DUB. Interestingly, they found that H2A deubiquitinase activity is required for proper transcriptional repression of Polycomb target genes *in vivo*. Furthermore, repression of Polycomb target genes is even more severely compromised if dRing, the E3 ligase for H2Aub, and PR-DUB are simultaneously depleted. Therefore, at least in *Drosophila*, complexes with directly opposing enzymatic activities on H2A synergistically regulate transcriptional repression. These results suggest that H2Aub in different genomic locations may have opposite influences on transcription or that dynamic cycles of H2A ubiquitylation and deubiquitylation may be required for proper gene repression. We look forward to studies that will investigate how the spatial, temporal, and kinetic control of H2Aub turnover on chromatin contributes to gene regulation. Such studies would greatly inform future *in vitro* studies using designer chromatin to more closely mimic the dynamism of histone ubiquitylation *in vivo*.

Finally, Richly *et al.* (40) identified ZRF1 as an H2Aub-binding protein involved in differentiation-dependent transcriptional activation of Polycomb target genes. If reduced PRC2 activity on Polycomb group-repressed genes is an important early step in pushing the chromatin state toward one more permissive to transcription, then our *in vitro* cross-talk data may provide another layer of mechanistic explanation for H2Aub involvement in transcriptional derepression.

Although our studies represent a significant advance in the use of designer nucleosomes containing H2Aub *versus* H2Bub, important uncertainties remain that will need to be addressed in future experiments. In particular, the role of ubiquitin turnover (*e.g.* due to the cyclic action of ubiquitin ligases and deubiquitinases) is not addressed in our system, nor are potential differences in spatial and temporal control of H2Aub and H3K27me in transcriptional regulation.

We look forward to subsequent studies that will use designer chromatin to explore enzymatic cross-talk relationships between H2Aub and H2Bub with not only MTases but also with other histone-modifying activities. More generally, we expect further study of histone PTM cross-talk relationships to be a fertile approach to understand how combinations of PTMs are coordinately regulated to maintain and affect dynamic changes in chromatin state, such as those that accompany gene expression changes resulting from developmental or environmental signal transduction.

Acknowledgments—We thank L. A. Banaszynski, C. M. Hughes, and J.-A. Kim for critical reading of the manuscript; R. Sadeh for helpful discussions; C. Chatterjee for help and guidance with preparing ssUb histones; and S. Wu and Y. Zhang for the generous contribution of the PRC2 complex.

REFERENCES

1. Kornberg, R. D. (1974) Chromatin structure: a repeating unit of histones and DNA. *Science* **184,** 868–871
2. Van Holde, K. E., Allen, J. R., Tatchell, K., Weischet, W. O., and Lohr, D. (1980) DNA-histone interactions in nucleosomes. *Biophys. J.* **32,** 271–282
3. Luger, K., Mäder, A. W., Richmond, R. K., Sargent, D. F., and Richmond, T. J. (1997) Crystal structure of the nucleosome core particle at 2.8 Å resolution. *Nature* **389,** 251–260
4. Kouzarides, T. (2007) Chromatin modifications and their function. *Cell* **128,** 693–705
5. Tan, M., Luo, H., Lee, S., Jin, F., Yang, J. S., Montellier, E., Buchou, T., Cheng, Z., Rousseaux, S., Rajagopal, N., Lu, Z., Ye, Z., Zhu, Q., Wysocka, J., Ye, Y., Khochbin, S., Ren, B., and Zhao, Y. (2011) Identification of 67 histone marks and histone lysine crotonylation as a new type of histone modification. *Cell* **146,** 1016–1028
6. Wang, Z., Zang, C., Rosenfeld, J. A., Schones, D. E., Barski, A., Cuddapah, S., Cui, K., Roh, T. Y., Peng, W., Zhang, M. Q., and Zhao, K. (2008) Combinatorial patterns of histone acetylations and methylations in the human genome. *Nat. Genet.* **40,** 897–903
7. Kharchenko, P. V., Alekseyenko, A. A., Schwartz, Y. B., Minoda, A., Riddle, N. C., Ernst, J., Sabo, P. J., Larschan, E., Gorchakov, A. A., Gu, T., Linder-Basso, D., Plachetka, A., Shanower, G., Tolstorukov, M. Y., Luquette, L. J., Xi, R., Jung, Y. L., Park, R. W., Bishop, E. P., Canfield, T. K., Sandstrom, R., Thurman, R. E., MacAlpine, D. M., Stamatoyannopoulos, J. A., Kellis, M., Elgin, S. C., Kuroda, M. I., Pirrotta, V., Karpen, G. H., and Park, P. J. (2011) Comprehensive analysis of the chromatin landscape in *Drosophila melanogaster*. *Nature* **471,** 480–485
8. Roudier, F., Ahmed, I., Bérard, C., Sarazin, A., Mary-Huard, T., Cortijo, S., Bouyer, D., Caillieux, E., Duvernois-Berthet, E., Al-Shikhley, L., Giraut, L., Després, B., Drevensek, S., Barneche, F., Dèrozier, S., Brunaud, V., Aubourg, S., Schnittger, A., Bowler, C., Martin-Magniette, M. L., Robin, S., Caboche, M., and Colot, V. (2011) Integrative epigenomic mapping defines four main chromatin states in *Arabidopsis*. *EMBO J.* **30,** 1928–1938
9. Briggs, S. D., Xiao, T., Sun, Z. W., Caldwell, J. A., Shabanowitz, J., Hunt,

D. F., Allis, C. D., and Strahl, B. D. (2002) Gene silencing: *trans*-histone regulatory pathway in chromatin. *Nature* **418,** 498
10. Dover, J., Schneider, J., Tawiah-Boateng, M. A., Wood, A., Dean, K., Johnston, M., and Shilatifard, A. (2002) Methylation of histone H3 by COMPASS requires ubiquitination of histone H2B by Rad6. *J. Biol. Chem.* **277,** 28368–28371
11. Ng, H. H., Xu, R. M., Zhang, Y., and Struhl, K. (2002) Ubiquitination of histone H2B by Rad6 is required for efficient Dot1-mediated methylation of histone H3 lysine 79. *J. Biol. Chem.* **277,** 34655–34657
12. Sun, Z. W., and Allis, C. D. (2002) Ubiquitination of histone H2B regulates H3 methylation and gene silencing in yeast. *Nature* **418,** 104–108
13. Santos-Rosa, H., Schneider, R., Bannister, A. J., Sherriff, J., Bernstein, B. E., Emre, N. C., Schreiber, S. L., Mellor, J., and Kouzarides, T. (2002) Active genes are trimethylated at K4 of histone H3. *Nature* **419,** 407–411
14. Schübeler, D., MacAlpine, D. M., Scalzo, D., Wirbelauer, C., Kooperberg, C., van Leeuwen, F., Gottschling, D. E., O'Neill, L. P., Turner, B. M., Delrow, J., Bell, S. P., and Groudine, M. (2004) The histone modification pattern of active genes revealed through genome-wide chromatin analysis of a higher eukaryote. *Genes Dev.* **18,** 1263–1271
15. McGinty, R. K., Kim, J., Chatterjee, C., Roeder, R. G., and Muir, T. W. (2008) Chemically ubiquitylated histone H2B stimulates hDot1L-mediated intranucleosomal methylation. *Nature* **453,** 812–816
16. Kim, J., Guermah, M., McGinty, R. K., Lee, J. S., Tang, Z., Milne, T. A., Shilatifard, A., Muir, T. W., and Roeder, R. G. (2009) RAD6-mediated transcription-coupled H2B ubiquitylation directly stimulates H3K4 methylation in human cells. *Cell* **137,** 459–471
17. Henry, K. W., Wyce, A., Lo, W. S., Duggan, L. J., Emre, N. C., Kao, C. F., Pillus, L., Shilatifard, A., Osley, M. A., and Berger, S. L. (2003) Transcriptional activation via sequential histone H2B ubiquitylation and deubiquitylation, mediated by SAGA-associated Ubp8. *Genes Dev.* **17,** 2648–2663
18. Pavri, R., Zhu, B., Li, G., Trojer, P., Mandal, S., Shilatifard, A., and Reinberg, D. (2006) Histone H2B monoubiquitination functions cooperatively with FACT to regulate elongation by RNA polymerase II. *Cell* **125,** 703–717
19. Tanny, J. C., Erdjument-Bromage, H., Tempst, P., and Allis, C. D. (2007) Ubiquitylation of histone H2B controls RNA polymerase II transcription elongation independently of histone H3 methylation. *Genes Dev.* **21,** 835–847
20. Xiao, T., Kao, C. F., Krogan, N. J., Sun, Z. W., Greenblatt, J. F., Osley, M. A., and Strahl, B. D. (2005) Histone H2B ubiquitylation is associated with elongating RNA polymerase II. *Mol. Cell. Biol.* **25,** 637–651
21. Wang, H., Wang, L., Erdjument-Bromage, H., Vidal, M., Tempst, P., Jones, R. S., and Zhang, Y. (2004) Role of histone H2A ubiquitination in Polycomb silencing. *Nature* **431,** 873–878
22. Nakagawa, T., Kajitani, T., Togo, S., Masuko, N., Ohdan, H., Hishikawa, Y., Koji, T., Matsuyama, T., Ikura, T., Muramatsu, M., and Ito, T. (2008) Deubiquitylation of histone H2A activates transcriptional initiation via *trans*-histone cross-talk with H3K4 di- and trimethylation. *Genes Dev.* **22,** 37–49
23. Ruthenburg, A. J., Li, H., Milne, T. A., Dewell, S., McGinty, R. K., Yuen, M., Ueberheide, B., Dou, Y., Muir, T. W., Patel, D. J., and Allis, C. D. (2011) Recognition of a mononucleosomal histone modification pattern by BPTF via multivalent interactions. *Cell* **145,** 692–706
24. Chatterjee, C., McGinty, R. K., Fierz, B., and Muir, T. W. (2010) Disulfide-directed histone ubiquitylation reveals plasticity in hDot1L activation. *Nat. Chem. Biol.* **6,** 267–269
25. McGinty, R. K., Köhn, M., Chatterjee, C., Chiang, K. P., Pratt, M. R., and Muir, T. W. (2009) Structure-activity analysis of semisynthetic nucleosomes: mechanistic insights into the stimulation of Dot1L by ubiquitylated histone H2B. *ACS Chem. Biol.* **4,** 958–968
26. Lowary, P. T., and Widom, J. (1998) New DNA sequence rules for high affinity binding to histone octamer and sequence-directed nucleosome positioning. *J. Mol. Biol.* **276,** 19–42
27. Cao, R., and Zhang, Y. (2004) SUZ12 is required for both the histone methyltransferase activity and the silencing function of the EED-EZH2 complex. *Mol. Cell* **15,** 57–67
28. Allis, C. D., and Muir, T. W. (2011) Spreading chromatin into chemical biology. *ChemBioChem* **12,** 264–279
29. Chatterjee, C., and Muir, T. W. (2010) Chemical approaches for studying histone modifications. *J. Biol. Chem.* **285,** 11045–11050
30. Böhm, L., Briand, G., Sautière, P., and Crane-Robinson, C. (1982) Proteolytic digestion studies of chromatin core histone structure. Identification of limit peptides from histone H2B. *Eur. J. Biochem.* **123,** 299–303
31. Böhm, L., Crane-Robinson, C., and Sautière, P. (1980) Proteolytic digestion studies of chromatin core histone structure. Identification of a limit peptide of histone H2A. *Eur. J. Biochem.* **106,** 525–530
32. Wu, L., Zee, B. M., Wang, Y., Garcia, B. A., and Dou, Y. (2011) The RING finger protein MSL2 in the MOF complex is an E3 ubiquitin ligase for H2B K34 and is involved in cross-talk with H3 K4 and K79 methylation. *Mol. Cell* **43,** 132–144
33. Goldknopf, I. L., and Busch, H. (1977) Isopeptide linkage between nonhistone and histone 2A polypeptides of chromosomal conjugate protein A24. *Proc. Natl. Acad. Sci. U.S.A.* **74,** 864–868
34. West, M. H., and Bonner, W. M. (1980) Histone 2B can be modified by the attachment of ubiquitin. *Nucleic Acids Res.* **8,** 4671–4680
35. Margueron, R., and Reinberg, D. (2011) The Polycomb complex PRC2 and its mark in life. *Nature* **469,** 343–349
36. Bernstein, B. E., Mikkelsen, T. S., Xie, X., Kamal, M., Huebert, D. J., Cuff, J., Fry, B., Meissner, A., Wernig, M., Plath, K., Jaenisch, R., Wagschal, A., Feil, R., Schreiber, S. L., and Lander, E. S. (2006) A bivalent chromatin structure marks key developmental genes in embryonic stem cells. *Cell* **125,** 315–326
37. Papp, B., and Müller, J. (2006) Histone trimethylation and the maintenance of transcriptional ON and OFF states by TrxG and PcG proteins. *Genes Dev.* **20,** 2041–2054
38. Schuettengruber, B., Chourrout, D., Vervoort, M., Leblanc, B., and Cavalli, G. (2007) Genome regulation by Polycomb and Trithorax proteins. *Cell* **128,** 735–745
39. Cloos, P. A., Christensen, J., Agger, K., and Helin, K. (2008) Erasing the methyl mark: histone demethylases at the center of cellular differentiation and disease. *Genes Dev.* **22,** 1115–1140
40. Richly, H., Rocha-Viegas, L., Ribeiro, J. D., Demajo, S., Gundem, G., Lopez-Bigas, N., Nakagawa, T., Rospert, S., Ito, T., and Di Croce, L. (2010) Transcriptional activation of Polycomb-repressed genes by ZRF1. *Nature* **468,** 1124–1128
41. Scheuermann, J. C., de Ayala Alonso, A. G., Oktaba, K., Ly-Hartig, N., McGinty, R. K., Fraterman, S., Wilm, M., Muir, T. W., and Müller, J. (2010) Histone H2A deubiquitinase activity of the Polycomb repressive complex PR-DUB. *Nature* **465,** 243–247
42. Eskeland, R., Leeb, M., Grimes, G. R., Kress, C., Boyle, S., Sproul, D., Gilbert, N., Fan, Y., Skoultchi, A. I., Wutz, A., and Bickmore, W. A. (2010) Ring1B compacts chromatin structure and represses gene expression independent of histone ubiquitination. *Mol. Cell* **38,** 452–464
43. Weake, V. M., and Workman, J. L. (2008) Histone ubiquitination: triggering gene activity. *Mol. Cell* **29,** 653–663
44. Minsky, N., Shema, E., Field, Y., Schuster, M., Segal, E., and Oren, M. (2008) Monoubiquitinated H2B is associated with the transcribed region of highly expressed genes in human cells. *Nat. Cell Biol.* **10,** 483–488
45. Shema, E., Tirosh, I., Aylon, Y., Huang, J., Ye, C., Moskovits, N., Raver-Shapira, N., Minsky, N., Pirngruber, J., Tarcic, G., Hublarova, P., Moyal, L., Gana-Weisz, M., Shiloh, Y., Yarden, Y., Johnsen, S. A., Vojtesek, B., Berger, S. L., and Oren, M. (2008) The histone H2B-specific ubiquitin ligase RNF20/hBRE1 acts as a putative tumor suppressor through selective regulation of gene expression. *Genes Dev.* **22,** 2664–2676

accurate information on prognosis is often difficult to obtain in this condition.

Conclusions

In general, CBT are associated with poor prognosis and only limited information is available at present due to a lack of sufficient cases. Diagnosis during fetal life is difficult. It is important to extensively evaluate the tumor on imaging (location, size and features) and clinical features (gestational age at diagnosis, complications) and select the most appropriate management of pregnancy and the perinatal treatment based on consultation with various specialists. Accumulation of further data is important to clarify the entire clinical picture and establish a management system for this condition.

References

1 Isaacs H. Perinatal brain tumors: A review of 250 cases. *Pediatr. Neurol.* 2002; **27**: 249–61.
2 Buetow PC, Smirniotopoulos JG, Done S. Congenital brain tumors: A review of 45 cases. *Am. J. Roentgenol.* 1990; **155**: 587–93.
3 Cassart M, Bosson N, Garel C, Eurin D, Avni F. Fetal intracranial tumors: A review of 27 cases. *Eur. Radiol.* 2008; **18**: 2060–66.
4 Im SH, Wang KC, Kim SK, Lee YH, Chi JG, Cho BK. Congenital intracranial teratoma: Prenatal diagnosis and postnatal successful resection. *Med. Pediatr. Oncol.* 2003; **40**: 57–61.
5 Carstensen H, Juhler M, Bøgeskov L, Laursen H. A report of nine newborns with congenital brain tumors. *Childs Nerv. Syst.* 2006; **22**: 1427–31.
6 Morita K, Fukuoka U, Kubota M *et al.* [A case of congenital brain tumor.] *Shounika Rinsho.* 2004; **57**: 1153–7. (in Japanese).
7 Cavalheiro S, Moron AF, Hisaba W, Dastoli P, Silva NS. Fetal brain tumor. *Childs Nerv. Syst.* 2003; **19**: 529–36.
8 Tamura M. Guidelines for healthcare provider and parents to follow in determining the medical care of newborns with severe diseases. *Saitama* 2004; **7**: 14–18.
9 ten Broeke ED, Verdonk GW, Roumen FJ. Prenatal ultrasound diagnosis of an intracranial teratoma influencing management: Case report and review of the literature. *Eur. J. Obstet. Gynecol. Reprod. Biol.* 1992; **45**: 210–14.

Vincristine, actinomycin D, cyclophosphamide chemotherapy resolves Kasabach–Merritt syndrome resistant to conventional therapies

Yasushi Fuchimoto,[1] Nobuyuki Morikawa,[3] Tatsuo Kuroda,[3] Seiichi Hirobe,[2] Shouichiro Kamagata,[2] Masaaki Kumagai,[4] Kentaro Matsuoka[5] and Yasuhide Morikawa[1]

[1]*Department of Surgery, Keio University School of Medicine,* [2]*Department of Surgery, Tokyo Metropolitan Children's Medical Center and Departments of* [3]*Surgery,* [4]*Hematology and* [5]*Pathology, National Center for Child Health and Development, Tokyo, Japan*

Key words infant, kaposiform hemangioendothelioma, Kasabach–Merritt syndrome, vincristine, actinomycin D and cyclophosphamide therapy.

When kaposiform hemangioendothelioma (KHE) is accompanied by Kasabach–Merritt syndrome (KMS), it may result in considerable morbidity and mortality.[1,2] The usual treatment for KHE associated with KMS of the extremities includes the use of steroids, coil embolization, radiation therapy and interferon-α. Recently, vincristine (VCR) has also been reported to be effective to control the coagulopathy in KMS.[2–5] In the present case, KMS was resistant to conventional therapies, and so we elected to use VCR monotherapy. Several courses of VCR monotherapy were insufficiently and transiently effective, and the consumptive coagulopathy recurred. Therefore, we decided to treat this patient using combined vincristine, actinomycin D and cyclophosphamide (VAC) therapy. After four cycles of VAC, KMS caused by the left arm hemangioma finally resolved and there has been no recurrence for 6 years. In this case, VAC therapy was effective after failure of repeated VCR monotherapy.

Correspondence: Yasushi Fuchimoto, MD, Department of Surgery, Keio University School of Medicine, 35 Shinanomachi, Shinjuku, Tokyo 160-8582, Japan. Email: yfuchimo@sc.itc.keio.ac.jp

Received 7 October 2010; revised 27 March 2011; accepted 13 May 2011.
doi: 10.1111/j.1442-200X.2011.03414.x

Case report

A male infant, born at full term by spontaneous vaginal delivery, was noted to have a large hemangioma of the left arm. He presented with anemia and thrombocytopenia at 1 month of age, and was diagnosed with KMS. The patient was referred to National Center for Child Health and Development for treatment of KMS at 2 months of age. First-line systemic therapy with corticosteroids was initiated (prednisolone 2 mg/kg per day) with simultaneous irradiation (10 Gy in five fractions), but it did not affect the tumor size or platelet counts. Subcutaneous injections of 1–3 × 10^6 (U/m^2 body surface area) of interferon-α for 1 month and mega-dose methylprednisolone therapy were then attempted, which also failed to improve KMS. At this stage the patient required 2 mg/kg per day of corticosteroids, and also needed frequent platelet transfusions to control bleeding. Transcatheter

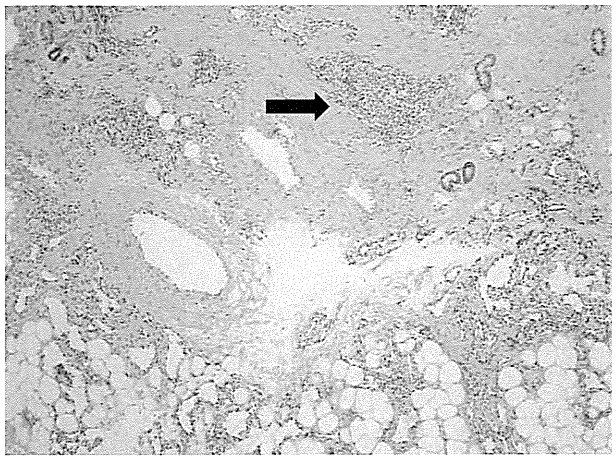

Fig. 1 Histopathology showing kaposiform hemangioendothelioma. The capillary vessels are diffusely proliferating in the fat tissues, and there is evidence of dense hyperplasia of the spindle shape cells (arrow).

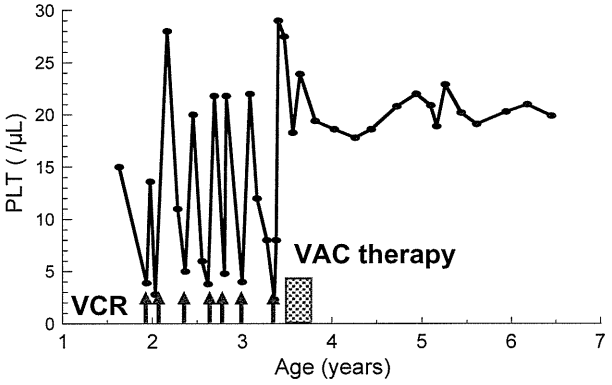

Fig. 3 Platelet counts after vincristine (VCR) or vincristine, actinomycin D and cyclophosphamide (VAC) therapy. VCR was dramatically effective for Kasabach–Merritt syndrome (KMS) but the effect was transient; the tumor showed regrowth and platelet counts repeatedly decreased. After eight courses of VCR monotherapy, the patient was treated with five courses of VAC. Remission of KMS was achieved for >4 years.

embolization of the feeding artery under general anesthesia was attempted three times. This resulted in a transient increase in the platelet counts. KMS relapsed within 2 weeks after the embolization. A biopsy showed that capillary vessels were diffusely proliferating in the fat tissues, and there was evidence of dense hyperplasia of spindle-shaped cells consistent with KHE, which frequently causes KMS (Fig. 1).[1,6–8]

Considering that the therapeutic effects of steroids, interferon-α, radiation, and embolization therapy were limited in the present case, we decided to start VCR. VCR was given weekly at a dose of 1.5 mg/m^2 (body surface area). After 8 weeks of VCR injections, the rate of platelet consumption gradually decreased, and platelet transfusions were no longer required (Fig. 2). After 11 cycles of VCR therapy, platelet counts increased up to 200 000/μL and were maintained at that level for a few months without any treatments. The tumor showed regrowth, however, and platelet counts decreased again 4 months after cessation of VCR therapy (Fig. 3). VCR monotherapy was again applied for recurrent KMS. In this situation, the platelet counts transiently increased after several episodes of VCR, but they gradually decreased after cessation of VCR therapy. After repeating seven doses of VCR monotherapy, at the age of 3 years it was decided to convert to a combination therapy of vincristine, actinomycin D, and cyclophosphamide (VAC). The VAC regimen included vincristine at 1.5 mg/m^2 on day 1, actinomycin D at 0.015 mg/kg on days 1–5 and cyclophosphamide at 10 mg/kg on days 1–3. During VAC therapy there were no serious side-effects. After four cycles of VAC therapy, KMS caused by the left arm hemangioma was finally resolved and there has been no recurrence for 6 years (Figs 3,4).

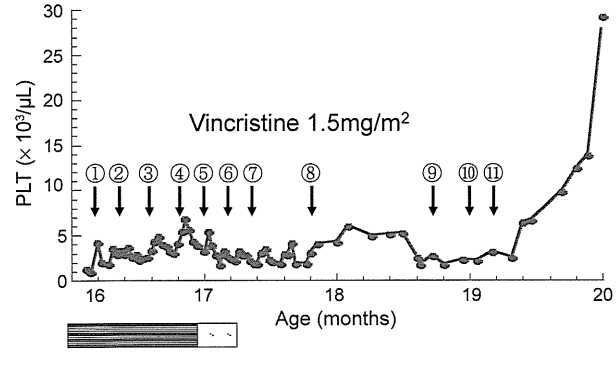

Fig. 2 Platelet (PLT) counts after vincristine (VCR) therapy. PLT infusions were required every day until the fifth VCR injection. After eight courses of VCR the patient did not require PLT infusions, and the PLT count increased from 40 000 to 250 000/μL.

Discussion

When KHE is accompanied by KMS, it may result in considerable morbidity and mortality. In the present case KMS was treated with steroids, coil embolization, radiation therapy and interferon-α, but these therapies were totally ineffective. Biopsy indicated KHE, which often causes life-threatening KMS.[9] Several reports have recently shown VCR to be effective for controlling the decreased platelet counts and potential mortality associated with KMS.[3–6,9–11] In addition, Haisley-Royster *et al.* reported that all four patients in whom KMS relapsed after a first course of VCR therapy, were successfully treated with second courses of VCR.[9] In contrast, the present patient had a relapse of KMS after several doses of VCR monotherapy.

Hu *et al.* reported that combined VAC therapy was effective for intractable KHE associated with KMS, which was resistant to corticosteroid therapy.[7] Because of toxicity considerations, such as veno-occlusive disease, hemorrhagic cystitis, pancytopenia

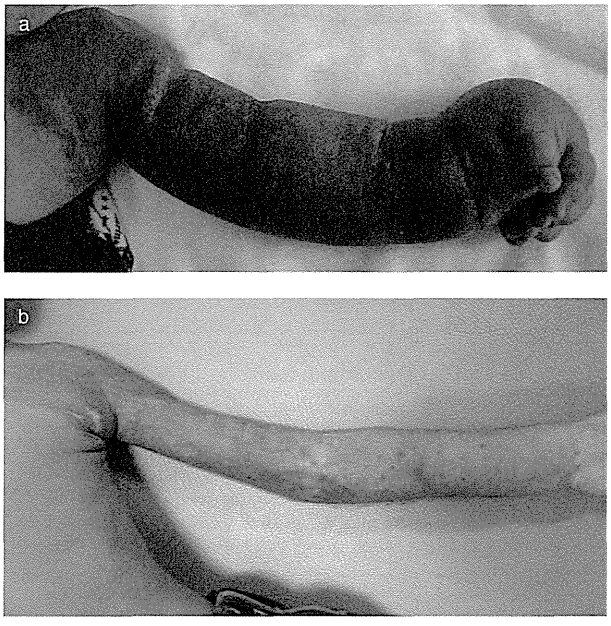

Fig. 4 (a) After six courses of vincristine there was a large, dark-red lesion covering the left arm and upper thorax. (b) After vincristine, actinomycin D and cyclophosphamide therapy, the dark-red lesion of the left arm had largely resolved.

and secondary malignancy, we were initially hesitant to use actinomycin D or cyclophosphamide. Only one case of KHE associated with KMS treated with VAC combination therapy after VCR monotherapy has been reported, but combination VAC chemotherapy was not effective in that report.[12] In addition, no comparative study of VAC combination therapy and VCR monotherapy for KHE associated with KMS has been reported. We decided to treat the present patient with VAC combination therapy because of the persistence of refractory coagulopathy and life-threatening condition.

Gottschling *et al.* reported that cyclophosphamide monotherapy was a safe and effective treatment for patients suffering from life-threatening diffuse hemangiomatosis unresponsive to corticosteroid therapy.[13] Cyclophosphamide monotherapy might have been effective in the present case but the previously reported cases all involved multiple cutaneous and liver hemangiomas, with complications that included high-output failure, and hepatic failure, and did not include KMS.

The present patient was treated with radiation therapy after steroid and interferon therapy. Due to problems with radiation therapy in infants, however, such as cancer or growth disorder, it might be better to treat pediatric patients with VCR or VAC chemotherapy prior to radiation therapy.

Vincristine, actinomycin D and cyclophosphamide therapy resulted in a significant decrease of tumor size, correction of the thrombocytopenia and a complete remission for 6 years in the present patient. The combined therapies of steroids, interferon-α, radiation and embolization were not effective for KHE in this patient. Thus, VAC therapy may provide an alternative therapeutic approach to intractable KMS resistant to conventional combination therapies, even when VCR monotherapy is not effective.

References

1 Enjolras O, Wassef M, Dosquet C *et al.* [Kasabach-Merritt syndrome on a congenital tufted angioma]. *Ann. Dermatol. Venereol.* 1998; **125**: 257–60.
2 Hall GW. Kasabach-Merritt syndrome: Pathogenesis and management. *Br. J. Haematol.* 2001; **112**: 851–62.
3 Moore J, Lee M, Garzon M *et al.* Effective therapy of a vascular tumor of infancy with vincristine. *J. Pediatr. Surg.* 2001; **36**: 1273–6.
4 Taki M, Ohi C, Yamashita A *et al.* Successful treatment with vincristine of an infant with intractable Kasabach-Merritt syndrome. *Pediatr. Int.* 2006; **48**: 82–4.
5 Thomson K, Pinnock R, Teague L, Johnson R, Manikkam N, Drake R. Vincristine for the treatment of Kasabach-Merritt syndrome: Recent New Zealand case experience. *N. Z. Med. J.* 2007; **120**(1249): U2418.
6 Yesudian PD, Klafkowski J, Parslew R, Gould D, Lloyd D, Pizer B. Tufted angioma-associated Kasabach-Merritt syndrome treated with embolization and vincristine. *Plast. Reconstr. Surg.* 2007; **119**: 1392–3.
7 Hu B, Lachman R, Phillips J, Peng SK, Sieger L. Kasabach-Merritt syndrome-associated kaposiform hemangioendothelioma successfully treated with cyclophosphamide, vincristine, and actinomycin D. *J. Pediatr. Hematol. Oncol.* 1998; **20**: 567–9.
8 Vin-Christian K, McCalmont TH, Frieden IJ. Kaposiform hemangioendothelioma. An aggressive, locally invasive vascular tumor that can mimic hemangioma of infancy. *Arch. Dermatol.* 1997; **133**: 1573–8.
9 Haisley-Royster C, Enjolras O, Frieden IJ *et al.* Kasabach-Merritt phenomenon: A retrospective study of treatment with vincristine. *J. Pediatr. Hematol. Oncol.* 2002; **24**: 459–62.
10 Fawcett SL, Grant I, Hall PN, Kelsall AW, Nicholson JC. Vincristine as a treatment for a large haemangioma threatening vital functions. *Br. J. Plast. Surg.* 2004; **57**: 168–71.
11 Perez J, Pardo J, Gomez C. Vincristine: An effective treatment of corticoid-resistant life-threatening infantile hemangiomas. *Acta Oncol.* 2002; **41**: 197–9.
12 Saito M, Gunji Y, Kashii Y *et al.* Refractory kaposiform hemangioendothelioma that expressed vascular endothelial growth factor receptor (VEGFR)-2 and VEGFR-3: A case report [Case Reports]. *J. Pediatr. Hematol. Oncol.* 2009; **31**: 194–7.
13 Gottschling S, Schneider G, Meyer S, Reinhard H, Dill-Mueller D, Graf N. Two infants with life-threatening diffuse neonatal hemangiomatosis treated with cyclophosphamide. *Pediatr. Blood Cancer* 2006; **46**: 239–42.

ELSEVIER

Pharmacokinetics of Mizoribine in Adult Living Donor Liver Transplantation

M. Shinoda, M. Tanabe, S. Kawachi, Y. Ono, T. Hayakawa, O. Iketani, M. Kojima, O. Itano, H. Obara, M. Kitago, T. Hibi, K. Matsubara, N. Shimojima, Y. Fuchimoto, K. Hoshino, G. Wakabayashi, M. Shimazu, Y. Tanigawara, T. Kuroda, Y. Morikawa, M. Kitajima, and Y. Kitagawa

ABSTRACT

We investigated the pharmacokinetics of mizoribine in the acute phase after adult living donor liver transplantation (LDLT). Between February 2004 and October 2009, 16 recipients received immunosuppressive therapy that included mizoribine (100 to 200 mg/d) after undergoing LDLT. We determined the serum levels of mizoribine before (C0) and 3 (C3), 4 (C4), and 10 (C10) hours after administration on postoperative days 3, 7, and 21. We assessed area under the concentration time curve (AUC) (hour · μg/mL), normalized serum concentration (NSC) at C0 [concentration (μg/mL)/dose (mg/kg body weight)], and estimated glomerular filtration rate (eGFR). The mizoribine concentration showed increases at C3 and C4 followed by a decrease at C10 on all days. AUC was 4.3, 5.9, and 8.3 in the 200-mg/d dose group on days 3, 7, and 21, respectively. NSC at C0 increased for 3 weeks after LDLT. There was a significant correlation between the NSC at C0 and eGFR on day 21, but not on days 3 and 7. There were no correlations between the NSC at C0 and either aspartate aminotransferase, total bilirubin, albumin, trough cyclosporine, or trough tacrolimus on any day. The pharmacokinetics of mizoribine in the acute phase after LDLT seems to be affected by postoperative day and renal function.

MIZORIBINE IS AN ORAL IMMUNOSUPPRESsive agent approved in Japan, Korea, and China for the prevention of graft rejection in renal transplantation. Its immunosuppressive potential is promising, and three-drug combination therapy with a calcineurin inhibitor, a steroid, and mizoribine is sometimes used for patients after renal transplantation.[1–3] The application of mizoribine has now been extended to lupus nephritis, chronic rheumatoid arthritis, and nephritic syndrome treatment in Japan.[4] Using antimetabolites as immunosuppressants in combination therapy may be beneficial for reducing the dose and side effects of calcineurin inhibitors or steroids after living donor liver transplantation (LDLT).[5,6] Due to the absence of information on the pharmacokinetics of mizoribine in liver transplantation, the options for secondary and tertiary agents in immunosuppressive combination therapy are limited to azathioprine (AZA) and mycophenolate mofetil (MMF). It is critical to ensure that the concentrations of the immunosuppressive agent used is maintained within an appropriate range, especially in the acute phase after LDLT, because even a minor failure in management postsurgically, when liver graft volume and function are not fully recovered, can be lethal. Since mizoribine is excreted from the kidneys, and since AZA and MMF are metabolized or activated in the liver, it is worthwhile to investigate the pharmacokinetics of these antimetabolites in patients with hepatic dysfunction. In this study, we monitored mizoribine levels on postoperative day 3, 7, and 21 and assessed the pharmacokinetics of mizoribine in the acute phase of LDLT.

From the Departments of Surgery (M.S., M.T., S.K., Y.O., M.K., O.I., H.O., M.K., T.H., K.M., Y.K.), Pharmacy (T.H., O.I., Y.T.), and Pediatric Surgery (N.S., Y.F., K.H., T.K., Y.M.), Keio University School of Medicine, Tokyo, Japan; Department of Surgery (G.W.), Iwate Medical University School of Medicine, Iwate, Japan; Department of Digestive Surgery (M.S.), Hachioji Medical Center of Tokyo Medical University, Tokyo, Japan; and International University Health and Welfare Mita Hospital (M.K.), Tokyo, Japan.

Masahiro Shinoda and Minoru Tanabe equally contributed to this study.

Address reprint requests to Minoru Tanabe, MD, PhD, Department of Surgery, Keio University School of Medicine, 35 Shinanomachi, Shinjuku-ku, Tokyo 160-8582, Japan. E-mail: m-tanabe@a6.keio.jp

0041-1345/–see front matter
http://dx.doi.org/10.1016/j.transproceed.2012.01.139

PATIENTS AND METHODS

Patients

Between February 2004 and October 2009, 16 transplant recipients were treated with an immunosuppressive regimen that included mizoribine after undergoing LDLT. The backgrounds of the patients are summarized in Table 1. The immunosuppressive regimen was a three-drug combination therapy. In cases of hepatitis C positivity, basiliximab was used instead of a steroid. In cases of ABO blood-type incompatibility, the three-drug combination therapy and additional regimens were employed; patients were preoperatively administered rituximab twice, and a steroid, prostaglandin El, and gabexate mesilate were administered through the portal vein for 3 weeks postoperatively. Mizoribine was given orally twice a day at a dose of 100 mg/d in the initial three cases, and 200 mg/d in the other 13 cases. Tacrolimus was chosen as the calcineurin inhibitor for the initial cases of hepatitis C positivity and ABO blood type incompatibility, and cyclosporine was used in the other cases.

Serum samples were collected before and 3, 4, and 10 hours after dosing on postoperative days 3, 7, and 21. All serum samples were analyzed to determine the mizoribine concentration. The concentrations before and 3, 4, and 10 hours postadministration were defined as C0, C3, C4, and C10, respectively. Blood samples were centrifuged for 5 minutes at 1500g, and all serum samples were stored at −80°C prior to being assayed. Informed consent was obtained from each patient or family, and the study protocol conformed to the ethical guidelines of Keio University School of Medicine.

Mizoribine Assay

Concentrations of mizoribine in serum were measured by Asahi Kasei Pharma Corporation (Tokyo, Japan) using high-performance liquid chromatography (HPLC). The serum was deproteinized and filtered (Ultra-Free C3LCC, Millipore, Tokyo). Filtrate (10 μL) was injected into an HPLC column (Shim-Pack CLC-NH2 15 cm × 6.0 mm internal diameter, Shimadzu, Kyoto). The mobile phase consisted of 66.7 mmol/L phosphate buffer (pH 2.5) and acetonitrile (27.5:72.5), and the flow rate was set at 1.3 mL/min. The drug was detected at a wavelength of 280 nm using a UV detector, and the detection limit was 0.02 μg/mL.

Table 1. Patient Background

Liver diseases	
Virus-related liver cirrhosis	11
Fulminant hepatitis	2
Primary biliary cirrhosis	2
Budd-Chiari syndrome	1
Sex	
Male	10
Female	6
Age (y)	49.5 ± 9.5
Body weight (kg)	60.6 ± 10.5
ABO blood type compatibility	
Identical	8
Compatible	4
Incompatible	4
Immunosuppressive regimen	
Cyclosporine, steroid, and mizoribine	8
Cyclosporine, basiliximab, and mizoribine	2
Tacrolimus, steroid, and mizoribine	2
Tacrolimus, basiliximab, and mizoribine	3
Cyclosporine to tacrolimus convert on day 14, steroid, and mizoribine	1
Mizoribine dose (minimum to maximum, mg/kg/day)	0.60–4.0

Blood Biochemistry

The serum levels of aspartate aminotransferase (AST), total bilirubin (TB), creatinine, albumin, and trough levels of cyclosporine and tacrolimus were determined by a biochemistry laboratory in our hospital.

Pharmacokinetic Parameters and Estimated Glomerular Filtration Rate

The area under the concentration-time curve (AUC) (hour · μg/mL) was estimated for the 100-mg/d dose patients, 200-mg/d dose patients, and all patients by summing three trapezoidal areas (C0 to C3, C3 to C4, and C4 to C10). Each trapezoid area was calculated by multiplying the concentration (μg/mL) by time (hours). The concentration of mizoribine was normalized according to dose and body weight using the following equation: [normalized serum concentration (NSC)] = [concentration of mizoribine (μg/mL)]/[dose of mizoribine (mg/kg)]. The area under the NSC-time curve [(hour · μg/mL)/(mg/kg)] was estimated for all patients by summing three trapezoidal areas (0 to 3 hours, 3 to 4 hours, and 4 to 10 hours). Each trapezoid area was calculated by multiplying the NSC [(μg/mL)/(mg/kg)] by time (hour). The highest concentration among C0, C3, C4, and C10 was defined as Cmax (μg/mL). The time from C0 to Cmax was defined as Tmax (hours). Clearance of mizoribine (Cl, L/h) was estimated by the following method: (1) elimination rate constant (kel) was calculated using the equation; kel ($hour^{-1}$) = −([natural logarithm of C10] − [natural logarithm of C4])/(10 − 4); (2) C12 was estimated using the equation: C12 = C10 × $\exp^{(-kel\times 2)}$; (3) the AUC of C0 to C12 was estimated by adding three trapezoidal areas (C0 to C3, C3 to C4, and C4 to C10) and one additional trapezoid (C10 to estimated C12); and (4) Cl was estimated using the equation; Cl (L/h) = [mizoribine dose per intake (mg)]/[estimated AUC of C0 to C12 (hour · μg/mL)]. The glomerular filtration rate (GFR) was estimated using the following equation: estimated GFR (eGFR, mL/min/1.73 m^2) = 194 × serum $creatinine^{-1.094}$ × $age^{-0.287}$ (if female, × 0.739).[7]

Adverse Events

A diagnosis of acute cellular rejection (ACR) was reached when patients showed elevation of hepatic enzymes and needle liver biopsy results showed more than moderate-grade ACR. Patients were diagnosed as having symptomatic infection if they had prolonged high fever and infection marker positivity (bacteria, cytomegalovirus, etc), or asymptomatic infection if they had the infection marker positivity without high fever. Patients were diagnosed as having hepatic dysfunction if they had reelevation of hepatic enzymes, and as having renal dysfunction if they underwent serum filtration.

Statistical Analysis

Results are expressed as means ± standard deviations (SDs) unless noted otherwise. For parametric data, differences between groups were evaluated using Student *t* test for unpaired data, based on the assumption that the data were derived from populations with equal SDs. Correlations were evaluated using the Spearman rank test. Differences were considered significant at *P* values less than .05.

RESULTS

Serum Mizoribine Concentrations

Figure 1a shows mean mizoribine concentrations in all patients in this study on postoperative days 3, 7, and 21. The levels were increased at C3 and C4 followed by a decrease at C10 on postoperative days 3, 7, and 21. The highest concentrations were 0.40, 0.65, and 0.90 μg/mL at C4 on postoperative days 3, 7, and 21, respectively. The C3/C0 ratios were 1.80 ± 0.73, 2.07 ± 1.68, and 1.94 ± 0.50 on postoperative days 3, 7, and 21; the respective C4/C0 ratios were 2.07 ± 1.33, 1.88 ± 1.14, and 1.79 ± 0.57, and the C10/C0 ratios were 1.54, 1.35, and 0.86. Figures 1b and 1c show mean mizoribine concentrations on postoperative days 3, 7, and 21 in the 200 and 100-mg/d dose groups,

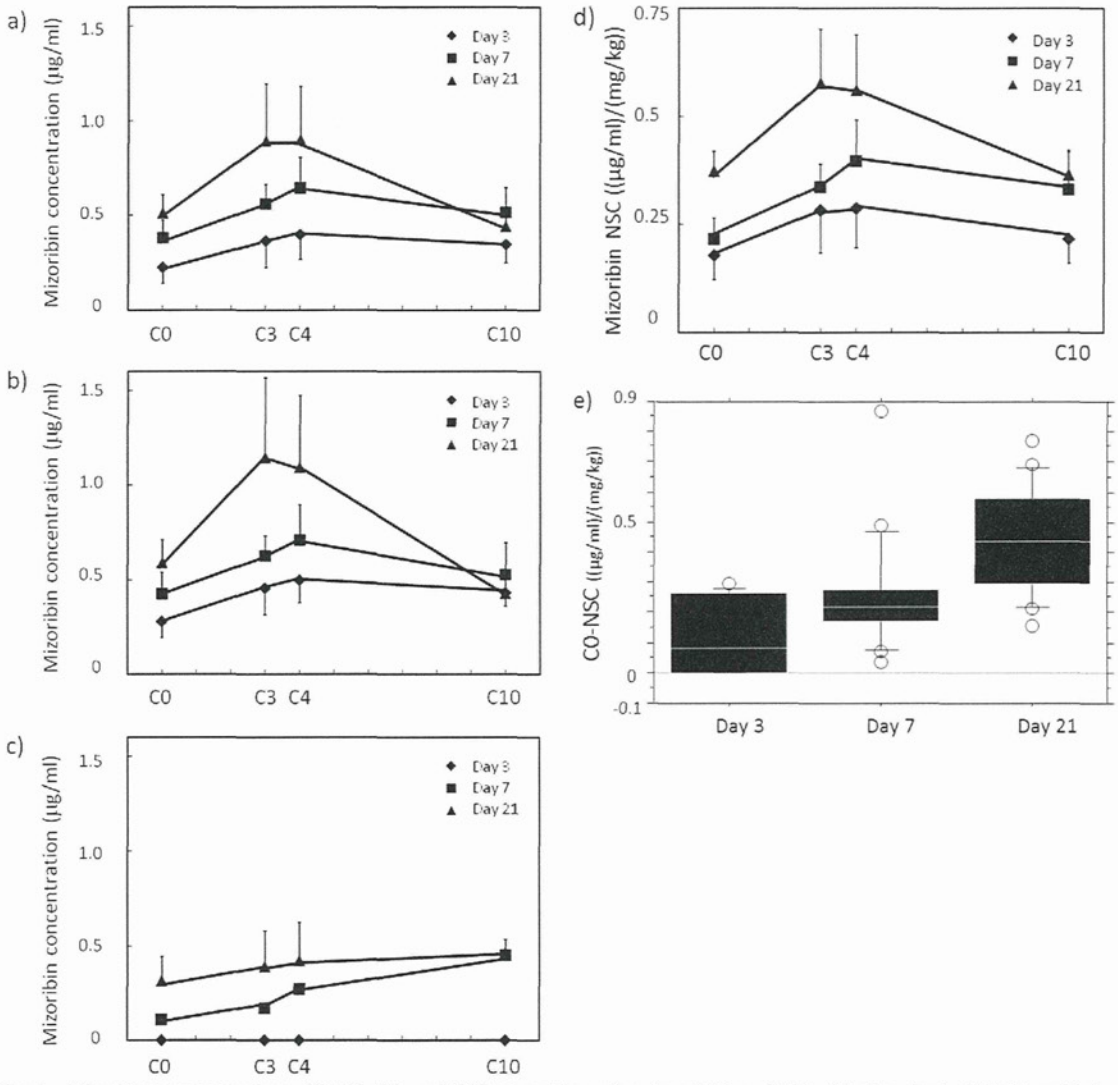

Fig 1. Mizoribine concentrations. C0, C3, C4, and C10 on postoperative days 3, 7, and 21 in (**a**) all patients, (**b**) 200-mg/d dose patients, and (**c**) 100-mg/d dose patients. (**d**) NSC at C0, C3, C4, and C10 on postoperative days 3, 7, and 21 in all patients. Results are expressed as mean + SEM or mean − SEM. C0, C3, C4, and C10; serum mizoribine concentration before and 3, 4, and 10 hours after mizoribine administration, respectively. (**e**) A quantile box plot of NSC at C0 on postoperative days 3, 7, and 21. The box for each day represents the interquartile range (25–75th percentile) and the line within this box is the median value. Bottom and top bars of the whisker indicate the 10th and 90th percentiles, respectively. Outlier values are indicated as open circles. NSC, normalized serum concentration; SEM, standard error of the mean.

respectively. Figure 1d shows NSC in all patients on postoperative days 3, 7, and 21. The NSC at C0 was increased in a time-dependent manner from day 3 to 21 and was significantly higher on postoperative day 21 compared to days 3 and 7 ($P < .05$; mean ± SD values of NSC at C0: 0.18 ± 0.14, 0.22 ± 0.14, and 0.37 ± 0.13 on days 3, 7, and 21, respectively). Figure 1e shows a quantile box plot of NSC at C0 on postoperative days 3, 7, and 21.

Pharmacokinetic Parameters

AUC, area under the NSC time curve, C0, Cmax, Tmax, and Cl are shown in Table 2. Results are expressed as mean ± SD. Maximum, median, and minimum values are indicated parenthetically in order.

Estimated Glomerular Filtration Rate

A quantile box plot of Fig 2 shows eGFR on postoperative days 3, 7, and 21. The mean ± SD eGFR values were 78 ± 23, 78 ± 31, and 64 ± 32 on days 3, 7, and 21, respectively. There were no significant differences among these values.

Effect of Parameters on Mizoribine Concentration

There was a significant correlation between the NSC at C0 and eGFR on day 21 (Fig 3c, $R^2 = 0.495$, $P < .05$), but not on days 3 and 7 (Fig 3a, 3b). There were no correlations between the NSC at C0 and either AST, TB, albumin, trough cyclosporine, or trough tacrolimus on any day (the R^2 values were extremely low and P values were >.05 in these analyses). There were no differences between the mizoribine trough NSCs at C0 in patients with tacrolimus and cyclosporine. There were no differences between the mizoribine trough NSCs at C0 in patients with and without steroids.

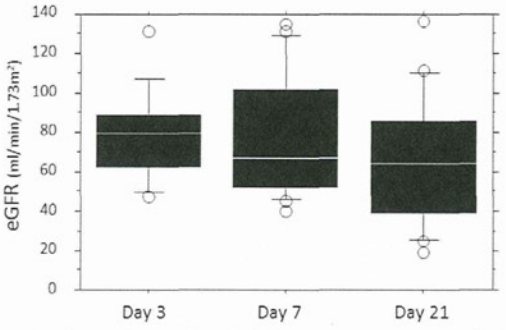

Fig 2. A quantile box plot of eGFR on postoperative days 3, 7, and 21. The box for each day represents the interquartile range (25–75th percentile) and the line within this box is the median value. Bottom and top bars of the whisker indicate the 10th and 90th percentiles, respectively. Outlier values are indicated as open circles. eGFR, estimated glomerular filtration rate.

Table 2. Pharmacokinetic Parameters

	100 mg/d	200 mg/d	All patients
Area under the concentration time curve (h · μg/mL)			
Postoperative day 3	0	4.3	3.4
Postoperative day 7	2.8	5.9	5.4
Postoperative day 21	4.1	8.3	7.0
Area under the NSC time curve [(h · μg/mL)/(mg/kg)]			
Postoperative day 3			2.4
Postoperative day 7			3.3
Postoperative day 21			4.7
C0 (μg/mL)			
Postoperative day 3	0 (0, 0, 0)	0.28 ± 0.19 (0.51, 0.38, 0.36)	0.22 ± 0.20 (0.51, 0.36, 0)
Postoperative day 7	0.18 ± 0.09 (0.24, 0.17, 0.11)	0.43 ± 0.28 (0.89, 0.35, 0.13)	0.36 ± 0.26 (0.89, 0.26, 0.11)
Postoperative day 21	0.34 ± 0.16 (0.47, 0.40, 0.16)	0.60 ± 0.26 (1.07, 0.56, 0.28)	0.52 ± 0.26 (1.07, 0.39, 0.16)
Cmax (μg/mL)			
Postoperative day 3	0 (0, 0, 0)	0.59 ± 0.22 (0.89, 0.61, 0.36)	0.59 ± 0.22 (0.89, 0.61, 0.36)
Postoperative day 7	0.35 ± 0.15 (0.45, 0.34, 0.24)	0.48 ± 0.50 (1.64, 0.59, 0.36)	0.66 ± 0.42 (1.64, 0.58, 0.24)
Postoperative day 21	0.49 ± 0.16 (0.67, 0.42, 0.38)	1.08 ± 0.82 (2.69, 0.83, 0.44)	0.88 ± 0.72 (2.69, 0.67, 0.38)
Tmax (h)			
Postoperative day 3		4.2 ± 4.1 (4, 3, 0)	4.2 ± 4.1 (4, 3, 0)
Postoperative day 7	5.0 ± 7.0 (10, 5, 0)	2.8 ± 1.4 (4, 3, 0)	3.4 ± 2.9 (10, 3, 0)
Postoperative day 21	5.6 ± 3.7 (10, 4, 3)	4.5 ± 2.7 (10, 3.5, 3)	4.8 ± 2.9 (10, 4, 3)
Cl (L/h)			
Postoperative day 3		20.7 ± 6.3 (28.2, 18.7, 12.7)	20.7 ± 6.3 (28.2, 18.7, 12.7)
Postoperative day 7	23.4 ± 14.4 (33.6, 23.4, 13.2)	18.0 ± 9.4 (30.1, 10.7, 7.1)	19.9 ± 9.7 (33.6, 19.2, 7.1)
Postoperative day 21	11.8 ± 4.3 (15.7, 12.6, 7.1)	14.3 ± 9.5 (30.4, 11.8, 5.1)	13.4 ± 7.6 (30.4, 12.2, 5.1)

NSC, normalized serum concentration; C0, serum mizoribine concentration before mizoribine administration; Cmax, highest concentration of serum mizoribine; Tmax, time from mizoribine administration to Cmax; Cl, clearance of mizoribine.

Adverse Events and Patient Outcomes

The incidence of adverse events is shown in Table 3. The seven cases of asymptomatic infection were patients who tested positive for cytomegalovirus infection but did not present with fever. All patients survived more than 3 weeks after operation.

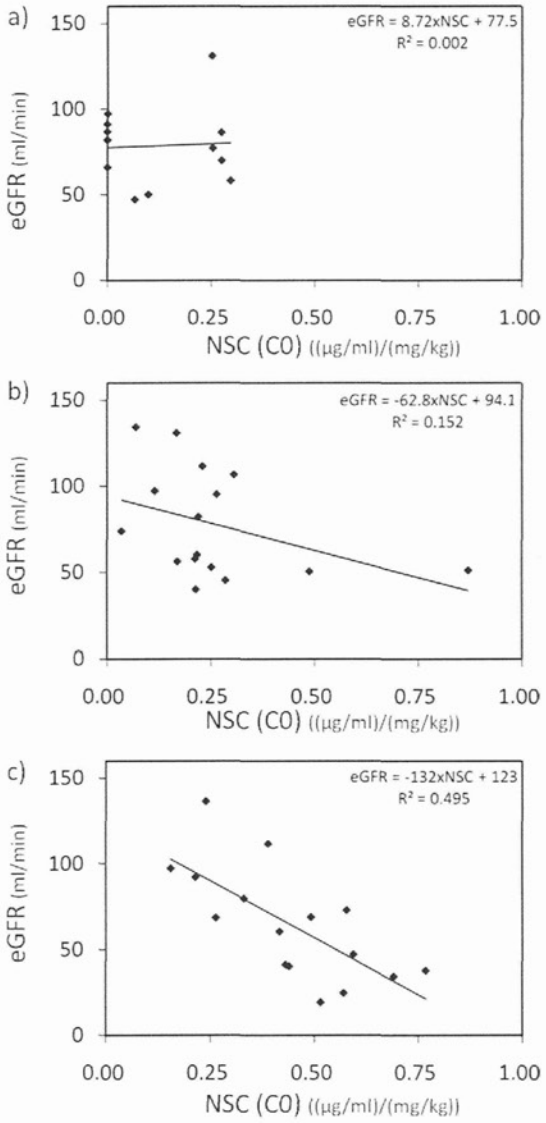

Fig 3. Correlation between mizoribine NSC at C0 and eGFR. Correlation between mizoribine NSC at C0 and eGFR on postoperative days 3 (**a**), 7 (**b**), and 21 (**c**). NSC, normalized serum concentration; eGFR, estimated glomerular filtration rate.

Table 3. Incidences of Adverse Events

	No. of cases
Mortality	0 (0%)
Antibody-mediated rejection	0 (0%)
Acute cellular rejection	1 (6%)
Central nervous disorder	1 (6%)
Hepatic dysfunction	1 (6%)
Pancytopenia	1 (6%)
Symptomatic infection	2 (12%)
Renal dysfunction	3 (18%)
Asymptomatic infection	7 (43%)

DISCUSSION

Our preliminary study in initial cases after LDLT showed that peak concentrations of mizoribine occurred 3 or 4 hours postadministration. Sugitani and colleagues reported that peak drug concentrations were reached approximately 3 hours after intake in patients who were treated with mizoribine more than 1 month after renal transplantation, at which time their condition had stabilized.[3] Therefore, we decided to collect serum samples before and 3, 4, and 10 hours after oral mizoribine administration to assess peak drug levels. The analysis showed that the highest concentration was 0.40, 0.65, and 0.90 μg/mL at C4 on postoperative days 3, 7, and 21, respectively, and the peak level was approximately twice the level at C0 on all days. Sugitani et al studied patients who took higher doses of mizoribine (4 to 6 mg/kg/d) and reported that the peak concentration was 2.87 μg/mL, the peak level was approximately twice the trough level, and there were few adverse events.[3] Our study employed LDLT patients who took lower doses of mizoribine (0.60 to 4.0 mg/kg/d) and showed that the peak concentrations were much lower than those reported by Sugitani et al. The lower concentrations in our study might be a result of not only the lower mizoribine dose used but also differences in intestinal absorption and renal excretion between subject populations. Since the incidence of adverse events in our study and that of Sugitani et al was acceptably low in both cases, a potential alternative mizoribine protocol for LDLT could include a higher dose of mizoribine to achieve higher trough and peak drug levels. However, the optimal serum concentration of mizoribine in organ transplantation patients has never been determined. In a study by Sonda et al, which employed the mixed lymphocyte reaction assay to assess the effects of mizoribine on peripheral lymphocytes from healthy adults, the inhibition rates were 2.4%, 36.4%, 43.8%, 52.6%, 62.2% at mizoribine concentrations of 0.05, 0.1, 0.5, 1.0, 5.0 μg/mL, respectively (8). According to these data, the drug doses used by Sugitani et al and in our study may have had an immunosuppressive effect on lymphocytes. Future clinical studies should determine the optimal serum concentration of mizoribine when it is used as a second or third agent in combination immunosuppressive therapy.

This study also showed that the NSC at C0 increased from postoperative day 3 to 21, suggesting that the NSC at

C0 did not reach a steady state until 3 weeks after the operation. The time to reach steady-state drug levels is generally calculated by multiplying the half-life of the drug by 3 to 5, if the excretion rate is stable. The half-life of mizoribine is 1.6 hours in patients with normal renal function (creatinine clearance > 70 mL/min) and 4.6 hours in patients with severely impaired renal function (creatinine clearance < 40 mL/min),[9] and it can be estimated that steady-state levels of mizoribine were reached within a few days postadministration in LDLT patients. The present finding that the NSC at C0 did not reach to a steady state until 3 weeks postoperatively suggests that the time to reach steady state was markedly prolonged in the LDLT patients. The pharmacokinetics of mizoribine depends on both intestinal absorption and renal excretion.[4] eGFR showed that levels were virtually unchanged on days 3 and 7 and slightly decreased on day 21. It is known that intestinal absorption is impaired in patients who have undergone long-duration laparotomy. Absorption may also be impaired in LDLT, which sometimes takes more than 10 hours to perform and involves major surgical procedures on the intestine. Therefore, we reason that the prolonged time to reach steady-state levels of mizoribine within 3 weeks after LDLT could be mainly attributable to poor absorption due to delayed gastric emptying and reduced intestinal motility following surgery. Recent studies have investigated the potential impact of bile flow[10] and the drug transporter of concentrative nucleoside transporter 1 polymorphisms[11] on mizoribine absorption. These factors might contribute to interindividual differences in the plasma disposition of mizoribine. Assessing the status of cholestasis in the liver and intestine of patients by measuring bile flow from biliary drainage tubes and genotyping for concentrative nucleoside transporter may provide additional insight into postoperative mizoribine absorption.

Because mizoribine is excreted by the kidneys, the serum concentration of mizoribine achieved during therapy should correlate with renal function. In fact, there was a significant relationship between trough NSC at C0 and eGFR on day 21. It is noteworthy that the correlation between NSC at C0 and eGFR was found only on day 21, but not on days 3 and 7. Sonda et al reported that the dose of mizoribine should be adjusted according to renal function in patients after renal transplantation.[8] We assume that this suggestion may not apply in the acute phase (several weeks) after LDLT because it may take time for mizoribine absorption to fully recover. It is reasonable that the serum concentration of mizoribine was independent of hepatic function represented by the hepatic markers of AST or TB, because mizoribine is neither metabolized nor activated in the liver. We investigated other possible factors that could be associated with mizoribine concentrations. One very important aspect and potential confounder in all pharmacokinetic studies after transplantation is the albumin concentration. However, mizoribine does not bind to proteins and, in fact, this study demonstrated that there was no relationship between trough NSC at C0 and albumin concentration on days 3, 7, and 21. Another aspect of interest is the impact of concomitant immunosuppressants such as steroids and calcineurin inhibitors on mizoribine concentrations. Hohage and colleagues reported that cyclosporine withdrawal resulted in a significant increase in the trough levels and AUC of mycophenolic acid in a group of renal transplant recipients with impaired renal function.[12] It is not known whether calcineurin inhibitors have a pharmacological effect on mizoribine concentrations. This study showed that there were no differences between the mizoribine trough NSCs at C0 in patients treated with tacrolimus and cyclosporine. Similarly, there were no differences between the mizoribine trough NSCs at C0 in patients with and without steroids. Therefore, this study did not find any factors associated with mizoribine concentration other than except renal function.

The efficacy and safety of mizoribine when used after LDLT is of great interest. Although mizoribine is now our preferred choice as a third agent in combination therapy, we previously used AZA or MMF as the third immunosuppressive agent together with a calcineurin inhibitor and a steroid in LDLT patients. It cannot be determined from this study if the immunosuppressive effect and incidence of adverse events with mizoribine are equivalent to those with AZA and MMF because the backgrounds of patients in whom mizoribine, AZA, and MMF were used are not comparable. We did not encounter lethal or severe adverse events arising from the use of mizoribine in this study. The finding that there was no relationship between NSC at C0 and AST or TB also provides information about the pharmacodynamics of mizoribine (ie, low-dose mizoribine may have a minimal adverse effect on hepatic function). Although our conclusions are limited by the small sample size in this study and a lack of comparative studies, it appears that low doses of mizoribine may be used safely after liver transplantation.

In the present study, we reported the pharmacokinetics of mizoribine in the acute phase after LDLT. The trend from C0 to C10 clearly showed that there were daily troughs and peaks, as was shown in a past study on renal transplantation by Sugitani and associates.[3] However, in our study both the peak and trough levels were much lower than those reported by Sugitani et al, probably because our protocol employed a relatively low dose of mizoribine. A new finding is that trough level increases for 3 weeks postoperatively. We assume that mizoribine adsorption is poor in the very early postoperative phase and, therefore, it takes 3 weeks until the serum concentration of this agent reaches a steady state. Mizoribine undergoes renal excretion, and its serum concentration should show a correlation with renal function if absorption is stable. It may not be possible to apply this correlation in the initial days following surgery, and a higher dose may be needed to compensate for poor absorption. The dose may need to be adjusted for renal excretion if more than 3 weeks passes after surgery. It is expected that mizoribine would have minimal adverse effects on hepatic function after surgery. Although there is

a period of poor mizoribine absorption in the very early postoperative phase, it could be a valuable alternative to agents that are metabolized or activated hepatically in cases where a renally excreted antimetabolite is preferable.

REFERENCES

1. Tanabe K, Tokumoto T, Ishikawa N, et al: Long-term results in mizoribine-treated renal transplant recipients: a prospective, randomized trial of mizoribine and azathioprine under cyclosporine-based immunosuppression. Transplant Proc 31:2877, 1999

2. Akiyama T, Okazaki H, Takahashi K, et al: Mizoribine in combination therapy with tacrolimus for living donor renal transplantation: analysis of a nationwide study in Japan. Transplant Proc 37:843, 2005

3. Sugitani A, Kitada H, Ota M, et al: Revival of effective and safe high-dose mizoribine for the kidney transplantation. Clin Transplant 20:590, 2006

4. Ishikawa H: Mizoribine and mycophenolate mofetil. Curr Med Chem 6:575, 1999

5. Jain A, Kashyap R, Dodson F, et al: A prospective randomized trial of tacrolimus and prednisone versus tacrolimus, prednisone and mycophenolate mofetil in primary adult liver transplantation: a single center report. Transplantation 72:1091, 2001

6. Eckhoff DE, McGuire BM, Frenette LR, et al: Tacrolimus (FK506) and mycophenolate mofetil combination therapy versus tacrolimus in adult liver transplantation. Transplantation 65:180, 1998

7. Matsuo S, Imai E, Horio M, et al: Revised equations for estimated GFR from serum creatinine in Japan. Am J Kidney Dis 53:982, 2009

8. Sonda K, Takahashi K, Tanabe K, et al: Clinical pharmacokinetic study of mizoribine in renal transplantation patients. Transplant Proc 28:3643, 1996

9. Koshikawa SSM, Narita K, Sakai K, et al: Clinical study of mizoribine on patients with incurable nephritic syndrome—a multicenter open study. Jin to Toseki 23:161, 1987

10. Mori N, Yokooji T, Kamio Y, et al: Increased intestinal absorption of mizoribine, an immunosuppressive agent, in cholestatic rats. Pharmazie 65:457, 2010

11. Naito T, Tokashiki S, Mino Y, et al: Impact of concentrative nucleoside transporter 1 gene polymorphism on oral bioavailability of mizoribine in stable kidney transplant recipients. Basic Clin Pharmacol Toxicol 106:310, 2010

12. Hohage H, Zeh M, Heck M, et al: Differential effects of cyclosporine and tacrolimus on mycophenolate pharmacokinetics in patients with impaired kidney function. Transplant Proc 37:1748, 2005

Pediatr Blood Cancer 2012;59:1332–1333

LETTER TO THE EDITOR
The Germline TP53 Mutation c.722 C>T Promotes Bone and Liver Tumorigenesis at a Young Age

To the Editor: Tumor protein 53 (TP53) is the most important tumor suppressor gene. The product of the gene p53 functions as a transcriptional factor, which is activated in response to a variety of physiological stresses and acts to halt deregulated cell proliferation [1]. TP53 mutations defining Li-Fraumeni syndrome (LFS) cause early onset of various different cancers [2]. Furthermore, some types of TP53 germline mutations cause specific problems. For example, Ribeiro et al. [3] reported that the germline point mutation encoding an R337H amino acid substitution is associated with pediatric adrenal cortical carcinomas in southern Brazil. DiGiammarino et al. [4] indicated that the mechanism of this phenomenon, a so-called genotype–phenotype correlation, could be explained by pH-dependent destabilization of a mutant p53 tetramer. Here, we report the third case of multiple cancers with the germline TP53 mutation c.722 C>T, which possibly involves a genotype–phenotype correlation.

An 8-year-old female with pain in her right knee was admitted to our hospital. Prior to admission, she had been healthy with no family history suggesting susceptibility to cancer. Magnetic resonance imaging showed an osteolytic tumor at the distal end of the femur. Whole-body imaging revealed a huge tumor in the liver, although no symptoms were observed. Plasma levels of alpha-fetoprotein were elevated up to 79,016 ng/ml. We performed biopsies for each site. Pathological findings from the sites were completely different. The biopsy specimen of the femur showed the proliferation of either polygonal or spindle-shaped tumorous cells with prominent osteoid tissue formation. In contrast, the liver tissue was dominated by large tumor cells with abundant eosinophilic cytoplasm, large vesiculated nuclei, and large nucleoli. Thus, her final diagnosis was osteosarcoma and hepatocellular carcinoma. Because she met the latest criteria for LFS [5], we examined her germline TP53 mutations by gene sequencing with the informed consent of her parents, although the parents themselves did not have testing. The results showed a germline missense mutation defined as c.722 C>T, p.Ser241Phe. We treated with chemotherapy combined with total resection of both tumors, and she has been disease-free for 13 months since completion of therapy.

According to The International Agency for Research on Cancer (IARC) database [6], this mutation has been previously identified in two children (Table I). As with our patient, they were diagnosed with multiple cancers before the age of 10 years, with no family history [7,8]. Only the parents of case 1 were confirmed as not having the mutation, because the other parents of case 2 and our patient were not tested. Furthermore, it is noteworthy that one of the two reported cases was affected by osteosarcoma and hepatoblastoma. There was no further information on case 2 other than the presence of two LFS core cancers. According to the IARC database, liver cancer has been reported only in two cases (0.17% of cancers associated with a TP53 germline mutation), whereas osteosarcoma is common. This suggests that c.722 C>T is a germline mutation promoting tumorigenesis in the bone and liver at a young age. Further reports of such cases will be required to confirm this conclusion.

Tomoo Osumi, MD
Masashi Miharu, MD
Hiroyuki Shimada, MD, PhD*
Department of Pediatrics
Keio University School of Medicine
Tokyo, Japan

Yasushi Fuchimoto, MD, PhD
Department of Pediatric Surgery
Keio University School of Medicine
Tokyo, Japan

Hideo Morioka, MD, PhD
Department of Orthopedic Surgery
Keio University School of Medicine
Tokyo, Japan

TABLE I. c.722 C>T TP53 Mutations in the Literature

Case	Proband cancer	Age at onset	Family history	Familial p53 mutation	Origin of mutation	Reference
1	Hepatoblastoma, osteosarcoma	3 months, 8 years	No cancer (parents, brother)	No mutation (parents, brother)	De novo germline	Toguchida et al. [7]
2	Two LFS core cancers	Concurrently under the age of 5	No cancer	Unknown	Unknown	Gonzalez et al. [8]
Our case	Hepatocellular carcinoma, osteosarcoma	Concurrently at the age of 8	No cancer (parents)	Unknown	Unknown	

*Correspondence to: Hiroyuki Shimada, MD, PhD, Department of Pediatrics, Keio University School of Medicine, 35 Shinanomachi, Shinjuku-ku, Tokyo 160-8582, Japan. E-mail: hshimada@a5.keio.jp

Received 26 March 2012; Accepted 3 July 2012

DOI 10.1002/pbc.24269
Published online 9 August 2012 in Wiley Online Library (wileyonlinelibrary.com).

Kenjiro Kosaki, MD, PhD
Center for Medical Genetics
Keio University School of Medicine
Tokyo, Japan

REFERENCES

1. Levine AJ. p53, the cellular gatekeeper for growth and division. Cell 1997;88:323–331.
2. Malkin D. Li-fraumeni syndrome. Genes Cancer 2011;2:475–484.
3. Ribeiro RC, Sandrini F, Figueiredo B, et al. An inherited p53 mutation that contributes in a tissue-specific manner to pediatric adrenal cortical carcinoma. Proc Natl Acad Sci USA 2001;98:9330–9335.
4. DiGiammarino EL, Lee AS, Cadwell C, et al. A novel mechanism of tumorigenesis involving pH-dependent destabilization of a mutant p53 tetramer. Nat Struct Biol 2002;9:12–16.
5. Tinat J, Bougeard G, Baert-Desurmont S, et al. Version of the Chompret criteria for Li Fraumeni syndrome. J Clin Oncol 2009;27:e108–e109 author reply e110.
6. The International Agency for Research on Cancer (IARC) TP53 database. http://www-p53.iarc.fr/
7. Toguchida J, Yamaguchi T, Dayton SH, et al. Prevalence and spectrum of germline mutations of the p53 gene among patients with sarcoma. N Engl J Med 1992;326:1301–1308.
8. Gonzalez KD, Buzin CH, Noltner KA, et al. High frequency of de novo mutations in Li-Fraumeni syndrome. J Med Genet 2009;46:689–693.

Ann Thorac Cardiovasc Surg Advance Published Date: August 20, 2012

doi: 10.5761/atcs.cr.11.01848

Case Report

Hepatoblastoma Metastasis Confined to the Pulmonary Artery: Report of a Case

Yotaro Izumi, MD,[1] Ken Hoshino, MD,[2] Naoki Shimojima, MD,[2] Yasushi Fuchimoto, MD,[2] Yuichiro Hayashi, MD,[3] Yasuhide Morikawa, MD,[2] and Hiroaki Nomori, MD[1]

Here, we report a case of hepatoblastoma metastasis to the left pulmonary artery which was resected by left lingular segmentectomy plus left lower lobectomy in 5-year-old girl. She had previously undertaken right upper lobectomy and multiple lung partial resections on bilateral lungs as hepatoblastoma metastatectomies. Prediction of postoperative pulmonary function based on perfusion scan merged with CT image and the measurement by CT volumetry, showed that left lingular segmentectomy plus left lower lobectomy could preserve 78% of the preoperative functional values and resection was done. Three weeks after the operation, her condition recovered to the preoperative level. Pathological examination showed that the metastasis was tumor embolism of hepatoblastoma which extended into the pulmonary arterial wall, which to our knowledge, has not been previously reported.

Keywords: hepatoblastoma, pulmonary metastasis, pulmonary metastasis

Introduction

Hepatoblastoma, along with hepatocellular carcinoma, is the most common malignant liver tumor in children and is the third most common childhood malignant abdominal tumor next to neuroblastoma and nephroblastoma.[1,2] Lung metastases of hepatoblastoma generally respond sufficiently to initial chemotherapy. The improvement of patient outcome with aggressive resection of lung metastases is not always achievable, particularly in cases in which metastases, which are not present at the time of diagnosis, appear during the course of treatment.[3] Nevertheless, resection is still the only treatment option for metastases which are refractory to chemotherapy. To this end, an accurate evaluation of the postoperative residual lung function is important, and surgical resection should be proactively considered if functionally feasible.

[1]*Division of General Thoracic Surgery, School of Medicine, Keio University, Tokyo, Japan*
[2]*Division of Pediatric Surgery, Department of Surgery, School of Medicine, Keio University, Tokyo, Japan*
[3]*Department of Pathology, School of Medicine, Keio University, School of Medicine, Keio University, Tokyo, Japan*

Received: November 21, 2011; Accepted: April 11, 2012
Corresponding author: Yotaro Izumi, MD. Division of General Thoracic Surgery, Department of Surgery, School of Medicine, Keio University, 35 Shinanomachi, Shinjuku-ku, Tokyo 160-8582, Japan
Email: yotaroizumi@a2.keio.jp

Case Report

A 5-year-old girl was diagnosed with hepatoblastoma by liver biopsy, pretreatment tumor extension 4, which was treated by systemic chemotherapy following the Japanese Study Group for Pediatric Liver Tumor-2 protocol. Response to chemotherapy 3 months later was progressive disease, and she underwent liver transplantation. Microscopic metastasis was detected in the perivascular tissue of the surgical margin of the hepatic vein. After liver transplantation, systemic irinotecan administration (20 mg/m2/day, days 1 to 5, and 8 to 12) was initiated but lung metastases developed.

In the period of 4 months following liver transplantation, left lung partial resection was done twice for each one metastasis, right lung partial resection was done once for 3 metastases, and right upper lobectomy for one

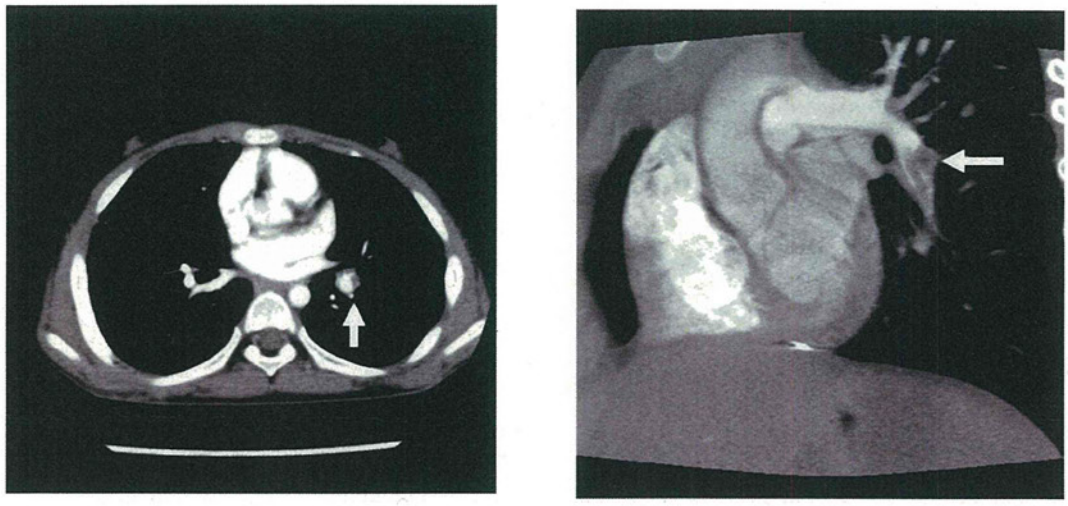

Fig. 1 A tumor was suspected in the left lung hilum on chest computed tomography (CT). (**A**) On contrast enhanced CT, hilar lymph node metastasis with invasion into the pulmonary artery was suspected. (**B**) Reconstructed sagittal view. The tumor resided predominantly inside the left basal pulmonary artery with possible extensions into A5 and A6.

A | B

metastasis was done along with systemic iritotecan administration. Six months after liver transplantation, serum level of alpha-fetoprotein (AFP) was elevated, 235 ng/ml (institutional standard value, under 20 ng/ml). On contrast enhanced computed tomography (CT), hilar lymph node metastasis with invasion into the pulmonary artery was suspected. The tumor resided predominantly inside the left basal pulmonary artery with possible extensions into A5 and A6 (**Fig. 1A** and **1B**). Lingula segmentectomy plus basal segmentectomy or lower lobectomy was planned. Her respiratory function was vital capacity (VC): 0.90 liters, percent of predicted normal VC (%VC) 78%, forced expiratory volume in 1 second (FEV1) 0.80 liters, and percent of predicted normal FEV1 (FEV1%): 89%. The predicted respiratory function after lingula segmentectomy plus lower lobectomy based on a simple calculation of the number of remaining segments was estimated to be approximately 60 % of the preoperative values (9 of 15 segments remaining).[4] Lung perfusion scan composed with CT images showed right lung to the left lung ratio of 1:0.78, with decreased flow to the left lower lobe, and lingula segment, 17%, and 5% of the total estimated pulmonary blood flow, respectively. Together with CT volumetry calculations, the respiratory function after lingula segmentectomy plus lower lobectomy was estimated to be approximately 78% of the preoperative values (VC: 0.72 liters, %VC: 61%, FEV1: 0.62 liters, FEV1: 69%). She was able to run the hospital corridor for at least 200 meters with sustained oxygen saturation by pulse oximetry at 98%. Since respiratory function prediction by subsegments counting has been reported to result in underestimation,[4] we collectively assessed that lingula segmentectomy plus lower lobectomy was tolerable in this patient.

Fifth rib bed thoracotomy was done, and the pleural adhesions from previous surgery were dissected. The left main pulmonary, A6a, A6b + c, A8 + 9 + 10, A4, and A5 were taped. The tumor was detected by ultrasound in the A8 + 9 + 10 basal pulmonary artery, but the exact extent could not be clearly depicted. No lesions were apparent in the lung or the left hilum, and the tumor seemed to be confined to the pulmonary arterial lumen. The blood flow of the interlobar pulmonary artery and its branches was tourniquet interrupted and an incision was made, on the distal part of A8 + 9 + 10, to visualize the tumor. Macroscopically, the tumor seemed to reside within the pulmonary vessel wall with extension into the vessel lumen. Proximally, the tumor extended beyond the bifurcation of A6 and A4 (**Fig. 2A** and **2B**). Preservation of the lingula segment or S6 was not considered possible, and left lingula segmentectomy plus lower lobectomy was done. On histology, tumor cells similar to the previously

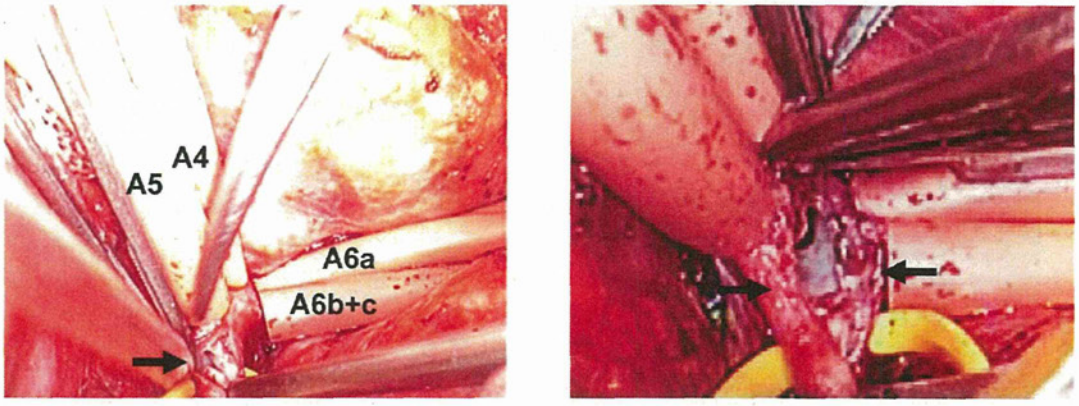

Fig. 2 Intraoperative findings. A vessel tourniquet was placed on the left A4, A5, A6a, and A6b + c. (**A**) The intravascular tumor was observed from the incision on the left basal pulmonary artery (arrow). (**B**) The incision on the left basal pulmonary artery was extended proximally. The tumor seemed to occupy not only the vessel lumen but also the vessel wall (arrows). The tumor extended proximal to the bifurcation of A6a and A4.

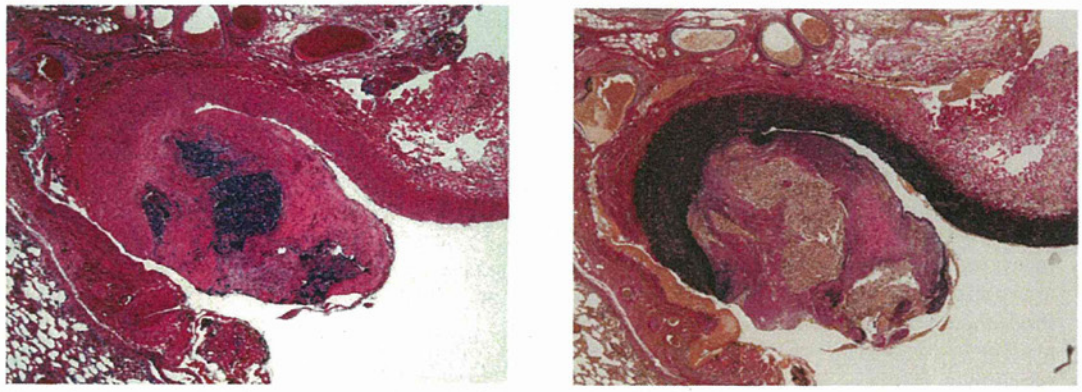

Fig. 3 Histological findings of the resected specimen. (**A**) On haematoxylin and eosin staining, tumor cells similar to the previously resected hepatoblastoma, were seen within an organized thrombi with extension into the vessel wall. (**B**) Elastica van Gieson staining showed that the internal elastic membrane of the vessel was intact, suggesting that the lesion was a tumor embolism, which extended into the vessel wall.

resected hepatoblastoma were seen within an organized thrombi with extension into the vessel wall (**Fig. 3A**). Elastica van Gieson staining showed that the vessel internal elastic membrane was intact (**Fig. 3B**). The cells present in the resected specimen appeared to be viable, and the effect of chemotherapy was considered to be marginal. The resected margin of the pulmonary artery was negative. Metastasis was not seen in the resected #11 lymph node. Tumor thrombus formation was not apparent in other regions of the resected specimen.

Mechanical ventilation was required for 7 days after surgery, but the patient regained preoperative performance status, i.e. 0, 3 weeks after surgery. Her respiratory function at 4 months after surgery was VC 0.80 liters, %VC 63%, FEV1 0.69 liters, FEV1% 92%, which was slightly better than the estimated postoperative respiratory function. Irinotecan was continued postoperatively. Tumor recurrence at the left lung hilum was suspected on CT 4 months after surgery. Although radiological changes due to surgical manipulation could not be completely ruled out,

taken together with the slightly elevated serum level of AFP (24 ng/ml), the lesion was irradiated. The left hilar lesion became undetectable after irradiation. Six months after surgery, the patient is without definitive residual disease, and serum AFP level is also normalized.

Discussion

The lung is known to be the most common site of metastasis for hepatoblastoma, but to our knowledge, metastasis confined to the pulmonary artery has not been reported. In the present case, the tumor was suspected to be tumor embolism which extended into the vessel wall. From the extent of the tumor in the present case, removal of the intravascular tumor followed by vessel plasty was considered to be insufficient, necessitating lung resection. The etiology of this metastasis is not clear, but as is frequently seen in hepatocellular carcinoma, the residual tumor at the hepatic vein margin may have somehow extended to the pulmonary circulation. To our knowledge, the impact of immunosuppression on the outcomes of liver transplantation for hepatoblastoma is still not established. As is in this patient, considering the exposure to chemotherapy throughout the course of treatment, it is possible that immunosuppression could be reduced in these patients thereby potentially decreasing the risk of recurrence as well as new malignancies.[5] To this end, further data accumulation is needed.

Since multiple pulmonary resections including a lobectomy had been previously performed on this patient, an accurate prediction of postoperative lung function was necessary. To this end, evaluation of lung perfusion scan fused with CT images, CT volumetry calculations,[6] and exercise capability, all proved to be very useful rather than resecting segments counting. The actual postoperative function was better than the predicted values. This could have been due to variances in the measurements, or may imply that compensatory lung growth occurred in this young patient.[7]

Disclosure Statement

None.

References

1) Matsunaga T, Sasaki F, Ohira M, et al. Analysis of treatment outcome for children with recurrent or metastatic hepatoblastoma. Pediatr Surg Int 2003; **19**: 142-6.
2) Perilongo G, Shafford EA. Liver tumours. Eur J Cancer 1999; **35**: 953-8; discussion 958-9.
3) Meyers RL, Katzenstein HM, Krailo M, et al. Surgical resection of pulmonary metastatic lesions in children with hepatoblastoma. J Pediatr Surg 2007; **42**: 2050-6.
4) Zeiher BG, Gross TJ, Kern JA, et al. Predicting postoperative pulmonary function in patients undergoing lung resection. Chest 1995; **108**: 68-72.
5) Suh MY, Wang K, Gutweiler JR, et al. Safety of minimal immunosuppression in liver transplantation for hepatoblastoma. J Pediatr Surg 2008; **43**: 1148-52.
6) Yoshimoto K, Nomori H, Mori T, et al. Prediction of pulmonary function after lung lobectomy by subsegments counting, computed tomography, single photon emission computed tomography and computed tomography: a comparative study. Eur J Cardiothorac Surg 2009; **35**: 408-13.
7) Nakajima C, Kijimoto C, Yokoyama Y, et al. Longitudinal follow-up of pulmonary function after lobectomy in childhood - factors affecting lung growth. Pediatr Surg Int 1998; **13**: 341-5.

Mixed chimerismによる免疫寛容誘導
大動物における前臨床研究と臨床応用

渕本康史*

特集 臓器移植臨床における免疫寛容導入の試みと現状

Induction of mixed chimerism and tolerance : A preclinical study in the large animal and clinical application

骨髄キメラによる免疫寛容誘導は最も安定した免疫寛容誘導法と考えられている．現在まで大動物では，ブタ，イヌ，サルにおいてmixed chimerismによる免疫寛容の研究に一定の成果を得ている．しかしキメラの安定性は動物種またはMHCバリアにより異なっている．ブタではMHCミスマッチ間においても安定したキメラが得られ，delayedの臓器移植にて免疫寛容を確認できている．サルではキメラは一過性であるが，臓器移植と骨髄移植を同時に行うことにより免疫寛容を得ている．Mixed chimerismを利用した臨床応用が開始されたが，ヒトではサルと同様に一過性のキメラであるが免疫寛容を一定の割合で得ることができている．サル，ヒトの場合は免疫寛容維持に移植臓器自体が関与していることが強く示唆される．

*Yasushi Fuchimoto**

key words：MC(mixed chimerism)，大動物，血液幹細胞移植，免疫寛容

新しい免疫抑制剤の開発により臓器移植の成績は飛躍的に改善した．しかし，移植臓器の長期生着に伴い慢性拒絶反応や免疫抑制剤の副作用が問題となっている．そのため免疫寛容は移植医療においてきわめて重要な課題であるが，免疫寛容においてはマウスなどの小動物の基礎研究が大動物で成功する例は少ない．

骨髄キメラ(chimerism)を利用した免疫寛容は最近臨床応用され成果を得ている数少ない寛容誘導法である．本稿では，骨髄キメラの大動物の前臨床研究から臨床への応用について述べる．

Mixed chimerismの基礎的概念

レシピエントの末梢血から成熟T細胞を除去したのちにドナーの血液幹細胞を注入することにより，骨髄においてドナーとレシピエントの両者の血液幹細胞の生着を成立させる．生着後は骨髄においてドナーとレシピエントの両者のmacrophageやB細胞といったantigen presenting cell(APC)が末梢に放出される．また胸腺においてはドナーとレシピエントの両者の樹状細胞が骨髄から胸腺の皮質-髄質境界部に移行し，そこでドナーとレシピエントの両者の抗原に高親和性のクローンが選択的に排除(clonal deletion)され，胸腺から末梢に放出されるT細胞は理論的にはドナーとレシピエントの両者に低反応となる(negative selection)．

免疫寛容には排除(deletion)，抑制(suppression)，麻痺(anergy)，無反応性(ignorance)などの機序があるが，mixed chimerism(以下MC)成立後の免疫寛容の機序は胸腺内での排除と考えられている[1,2](図1)．

マウスの研究から大動物の研究へ

前述のごとく，マウスにおいてはMCを含め，多くのドナー特異的免疫寛容を誘導する方法が報告されている．しかし，これらの方法の大部分が

*Department of Surgery, National Center for Child Health and Development 独立行政法人国立成育医療研究センター臓器・運動器病態外科部外科